An Investigation of the Plastic Fracture of AISI 4340 and 18 Nickel--200 Grade Maraging Steels

T. B. COX AND J. R. LOW, JR.

The mechanisms of plastic fracture (dimpled rupture) in high-purity and commercial 18 Ni, 200 grade maraging steels and quenched and tempered AISI 4340 steels have been studied. Plastic fracture takes place in the maraging alloys through void initiation by fracture of titanium carbo-nitride inclusions and the growth of these voids until impingement results in coalescence and final fracture. The fracture of AISI 4340 steel at a yield strength of 200 ksi (1378 MN/mm^2) occurs by nucleation and subsequent growth of voids formed by fracture of the interface between manganese sulfide inclusions and the matrix. The growth of these inclusion-nucleated voids is interrupted long before coalescence by impingement, by the formation of void sheets which connect neighboring sulfide-nucleated voids. These sheets are composed of small voids nucleated by the cementite precipitates in the quenched and tempered structures. The sizes of non-metallic inclusions are an important aspect of the fracture resistance of these alloys since the investigation demonstrates that void nucleation occurs more readily at the larger inclusions and that void growth also proceeds more rapidly from the larger inclusions. Using both notched and smooth round tensile specimens, it was demonstrated that the level of tensile stress triaxiality does not effect the void nucleation process in these alloys but that increased levels of triaxial tension do result in greatly increased rates of void growth and a concomitant reduction in the resistance to plastic fracture.

RECENTLY, increased use has been made of high-strength alloy steels for critical structural applications in naval vessels, air craft, and aerospace vehicles. Unlike the low-strength ferritic steels in which unstable brittle fracture occurs by cleavage, these high-strength alloys may fracture in a brittle manner by dimpled rupture due to highly localized, severe plastic deformation.[1] While brittle fracture of steels by cleavage has been extensively studied and many of the microstructural features which affect cleavage have been determined, very little research has been done on the plastic fracture process (frequently referred to as dimpled rupture, fibrous fracture, or ductile fracture) since, in the past, it generally occurred in a very ductile manner without catastrophic results.

There are three generally recognized stages of plastic fracture: void initiation, void growth, and void coalescence. It is usually observed that the initiation of voids at second-phase particles within the metal matrix is the first step in the plastic fracture process.[2] The subsequent growth and coalescence of these voids during further loading eventually leads to final fracture. An extensive study using copper alloys with various second-phase particles including metals, nonmetals, and voids by Edelson and Baldwin[3] showed that the ductility of the aggregates increased as the volume fraction of any of the second-phase particles was reduced. The improvement in ductility was extremely rapid with reductions in volume fractions of second-phase at and below about 0.01, a level approximately that found in most commercial alloys. It has been demonstrated that lowering the sulfur content of pearlitic steels can result in substantial improvements in the energy level of the upper Charpy shelf,[4] and reduced sulfur levels in quenched and tempered steels has also been shown to improve fracture toughness.[5] While the practical method of improving the fracture toughness of the high-strength steels by reducing the impurity levels is based upon these observations, very little is understood concerning the mechanisms of the plastic fracture process in the high-strength alloys.

The objectives of this investigation were to describe the mechanisms by which several common high-strength steels fracture plastically, with the belief that through a better understanding of the fracture process, it would be possible to suggest means of improving the resistance of these alloys to fracture. Determination of the reasons for the brittle nature of plastic fractures when occurring under high levels of triaxial tension was also an objective of this research, together with an explanation for the generally observed fact that the maraging steels exhibit much higher fracture toughness values than the quenched and tempered steels when compared at equal strength levels.

MATERIALS

The materials used in this investigation included both high-purity and commercial heats of AISI 4340 steel and 18 Ni, 200 grade maraging steel provided in plate form. The chemical analyses of the four alloys are presented in Table I. The major differences to be noted are the substantial reductions in impurity

T. B. COX is Metallurgist, Code 2811 Metals Division, Naval Ship Research and Development Center, Annapolis, Md. 21402. J. R. LOW, Jr., is Professor, Department of Metallurgy and Materials Science, at Carnegie-Mellon University, Pittsburgh, Pa. 15213.

Manuscript submitted July 9, 1973.

levels in the high-purity heats compared to the commercial heats.

Since it was desired to investigate the fracture behavior of these alloys at approximately the same strength level, they were given heat treatments designed to produce yield strengths close to 200 ksi (1378 MN/mm^2). Both AISI 4340 alloys were austenitized at 843°C (1550°F) for one hour and oil quenched. Due to the differences in carbon contents, the tempering treatments were different with the commercial AISI 4340 being tempered at 435°C (815°F) for one hour and air cooled while the high-purity alloy was tempered at 427°C (800°F) for one hour and air cooled. The specially produced high-purity 18 Ni, 200 grade maraging steel was solution annealed at 843°C (1550°F) for one hour and water quenched, then aged for three hours at 454°C (850°F) and air cooled. The commercial grade 18 Ni steel was solution annealed at 899°C (1650°F) for two and one-half hours and air cooled, followed by aging at 446°C (835°F) for six hours and air cooled.

The room temperature mechanical properties resulting from these heat treatments are given in Table II. The tensile data were determined using standard geometry, smooth, round tensile specimens; and the fracture toughness testing was carried out using both compact tension specimens and bend specimens in accordance with ASTM Standard E399-72. The fracture toughness specimens were tested in the TL orientation (notched through the plate thickness with the direction of crack propagation in the primary rolling direction). The tension test specimens were cut from the plates with the tension axis lying in the plane of the plate and perpendicular to the primary rolling direction, that is, with the direction of the tension axis in the same orientation as the principle normal stress in the fracture toughness specimens.

Reference to Table II reveals that the yield strengths of the alloys are in the general range of 200 ksi (1378 MN/mm^2). The values of true strain to fracture (reduction in area) indicate that the ductility of these alloys is substantially improved by high-purity melting, and that the general level of ductility is higher for the maraging steels than for the quenched and tempered AISI 4340 alloys. Also, the level of fracture toughness is greater in the maraging steels than in the AISI 4340 steels even when considering the differences in yield strengths. Within a given alloy system, reduction of the impurity levels improves the fracture toughness.

Table I. Chemical Composition of High Strength Steels (Wt Pct)

	Commercial AISI 4340	High Purity AISI 4340	Commercial 18 Ni	High Purity 18 Ni
C	0.43 ± 0.01	0.38 ± 0.01	0.021 ± 0.004	0.002 ± 0.002
Mn	0.78 ± 0.02	0.71 ± 0.02	0.04 ± 0.001	<0.02 ± 0.01
P	0.010 ± 0.001	0.001 ± 0.001	0.003 ± 0.001	0.002 ± 0.001
S	0.013 ± 0.001	0.004 ± 0.001	0.008 ± 0.001	0.004 ± 0.001
Si	0.27 ± 0.02	0.29 ± 0.02	0.04 ± 0.01	<0.03 ± 0.02
Ni	1.73 ± 0.02	1.81 ± 0.02	18.3 ± 0.1	18.1 ± 0.1
Cr	0.76 ± 0.02	0.80 ± 0.02	<0.04 ± 0.02	0.05 ± 0.02
Mo	0.25 ± 0.01	0.25 ± 0.01	4.23 ± 0.05	4.16 ± 0.05
Al(total)	0.049 ± 0.003	0.023 ± 0.002	0.080 ± 0.002	0.062 ± 0.002
Co	–	0.010 ± 0.01	7.85 ± 0.1	8.03 ± 0.1
Ti	–	<0.005 ± 0.002	0.19 ± 0.01	0.23 ± 0.01
N_2	0.008 ± 0.001	0.003 ± 0.001	0.005 ± 0.001	0.004 ± 0.001
O_2	50 ± 10 ppm	23 ± 3 ppm	30 ± 10 ppm	23 ± 3 ppm
Fe	Balance	Balance	Balance	Balance

Table II. Room Temperature Mechanical Properties of High Strength Steels (All Values Represent Means of Duplicate Tests)

	Commercial AISI 4340	High Purity AISI 4340	Commercial 18 Ni	High Purity 18 Ni
Yield Strength 0.2 pct Offset (ksi) (1 ksi = 6.89 MN/mm^2)	204.8	204.6	193.5	189.9
Ultimate Tensile Strength (ksi) (1 ksi = 6.89 MN/mm^2)	221.6	218.0	197.7	198.5
True Strain to Fracture	0.287	0.515	0.747	1.005
Fracture Toughness K_{Ic} (ksi $\sqrt{in}$) (1 ksi $\sqrt{in}$ = 1.10 MN $\sqrt{m}$/m^2)	67.9	97.2	113.0	149.1*

*K_Q, invalid test due to undersized specimens. All specimens were nominally 1 in (2.54 cm) thick.

NON-METALLIC INCLUSIONS

As indicated above, past investigators have noted that in many instances non-metallic inclusions are the sites for void nucleation. In order to define the exact nature of the non-metallic inclusions in these four alloys, a metallographic investigation was carried out. For each of the four alloys, metallographic sections were examined from each of three orthogonal directions, the axes being defined by the rolling directions and the through thickness direction in each of the plates.

Polished sections of both commercial and high-purity AISI 4340 alloys revealed that the predominate inclusion type in these alloys appeared as a gray ellipse in each of the three perpendicular directions. Generally, the inclusions were observed to be larger in the commercial AISI 4340, and the major axes of the ellipses seemed more elongated in the rolling direction of the commercial alloy. Examination of these inclusions, using a scanning electron microscope equipped with an X-ray energy-dispersive analyzer, showed that the ellipsoidal inclusions in both the commercial and high-purity AISI 4340 alloys were much richer in manganese and sulfur than the matrix while small irregular particles generally found within the ellipsoids were shown to contain calcium and aluminum. Based upon these X-ray data and their appearance in the optical microscope as compared with descriptions from previous inclusion studies,[6] these gray, ellipsoidal inclusions in the AISI 4340 alloys were identified as manganese sulfides (MnS); and the dark particles internal to the sulfides as some product of the deoxidation process upon which the sulfides are nucleated.

The most prevalent non-metallic inclusion type in both of the 18 Ni, 200 grade maraging alloys appeared as sections of cubes and exhibited a pink color in the optical microscope in all three views. The cubes did not appear to have been plastically deformed during the hot-rolling operation, and the cubic sections ap-

peared to have approximately the same size distribution in each of the three views of a given alloy. The cubes did appear to be larger in the commercial 18 Ni maraging steel. Comparison of these optical metallographic observations with those of a previous investigation[7] together with X-ray data from the scanning electron microscope showing that the cubes were rich in titanium identified these inclusions as titanium carbo-nitrides, Ti(C,N).

A quantitative metallographic investigation using light microscopy was undertaken to determine the exact nature of the inclusion populations in the four alloys. Based on the definition of the inclusion shapes indicated above, established quantitative metallographic techniques were used to determine the numbers, spacings, sizes, and volume fractions of the inclusions in the alloys. The quantitative metallographic analysis for the manganese sulfide ellipsoids is due to DeHoff and Rhines[8,9] and the analysis for the titanium carbo-nitride cubes is due to Hull and Houk.[10] The results of the quantitative metallography are summarized in Table III where the limits given for each reported value represent plus and minus one standard deviation. While a few inclusion types other than the manganese sulfides and titanium carbo-nitrides were occasionally observed, they were too few in number to be statistically significant and apparently did not affect the fracture process as demonstrated below.

It should be noted in Table III that the number of inclusions per unit volume (N_v) is greater for the high-purity alloys than for the commercially produced plates, but that inclusion sizes ($\bar{d}_1$, $\bar{d}_2$, $\bar{d}_3$ represent the average diameters of the ellipsoidal manganese sulfides and $\bar{a}$ the average cube edge of the titanium carbo-nitrides) and volume fractions (V_v) are substantially larger in the commercial alloys. Note also that the volume fractions of inclusions in the maraging steels are larger than in the AISI 4340 alloys even though the maraging alloys are tougher (see Table II). The center-to-center spacings of inclusions ($\bar{\lambda}$) follow the inverse relation of the number per unit volume, namely the interparticle spacings are greater in the commercial alloys than in the high purity alloys. As may be seen from the results, the variability of the various measurements is quite high. However, treatment of the data using standard statistical methods for hypotheses concerning means shows that the above conclusions concerning numbers, sizes, spacings, and volume fractions of the inclusions are statistically meaningful with 90 pct confidence.

FRACTOGRAPHY

A fractographic study was carried out on the four alloys to define the nature of the fracture surfaces. The fracture surfaces from plane strain fracture toughness specimens, smooth, round tensile bars, and mildly notched tensile bars were examined for each alloy. All of the fracture surfaces on the fracture toughness specimens were rough and fibrous in appearance when viewed at low magnification. Both the smooth and notched round tensile bars for all alloys exhibited a cup and cone type fracture with the central regions being rough and fibrous in appearance at low magnifications.

Two stage, cellulose acetate–platinum shadowed carbon replicas were taken from the areas of fast fracture initiation on the K_{Ic} fracture surfaces and from the central areas of normal rupture on the smooth and notched tensile fracture surfaces for each of the alloys. The replicas were examined using an electron microscope, and based upon extensive examination of stereo pairs, it was found that the features on the fracture surfaces were qualitatively the same for each of the three fracture tests (K_{Ic}; smooth, round tension; and notched, round tension) of any given alloy. All the fractures were entirely by dimpled rupture (plastic fracture).

Quantitative measurements of the sizes and spacings of dimples on many fracture surfaces revealed that the average spacings of large dimples corresponded well with the center-to-center spacings of the predominate non-metallic inclusions in each of the alloys. Furthermore, these measurements confirmed the observation that the features on the fracture surfaces were the same for the three specimen geometries for any given alloy. Thus, it is suggested that the microstructural processes which lead to fracture are the same for all three tests in these particular alloys even though the level of constraint (stress triaxiality) increases substantially when going from a smooth, round specimen to a notched, round specimen to a fatigue cracked plane strain specimen. It is important to note that stereoscopy was used extensively to determine the exact nature and extent of the dimples on the fracture surfaces. Incorrect conclusions can be reached concerning the features on fracture surfaces if planar micrographs are used alone without the aid of a stereo viewer, as demonstrated by Broek.[36]

An example of a typical fractograph taken from the 18 Ni, 200 grade maraging steels is presented in Fig.

Table III. Results of Quantitative Metallographic Investigation of Inclusions in High Strength Steels

	Commercial AISI 4340	High Purity AISI 4340	Commercial 18 Ni Maraging	High Purity 18 Ni Maraging
N_v (inclusions/cm^3)	$4.9 \times 10^6 \pm 2.6 \times 10^6$	$6.8 \times 10^6 \pm 4.6 \times 10^6$	$2.9 \times 10^6 \pm 1.5 \times 10^6$	$5.4 \times 10^6 \pm 5.1 \times 10^6$
$\bar{d}_1$ or $\bar{a}$ (μm)	9.7 ± 5.8	4.5 ± 4.1	8.6 ± 6.4	3.0 ± 3.8
$\bar{d}_2$ (μm)	7.3 ± 6.3	4.9 ± 4.2	–	–
d_3 (μm)	5.5 ± 1.4	3.3 ± 0.2	–	–
$\bar{\lambda}$ (μm)	33 ± 6	29 ± 7	39 ± 7	32 ± 10
V_v (pct)	0.14 ± 0.05	0.06 ± 0.03	0.21 ± 0.08	0.09 ± 0.05

Note: $\bar{d}_i$ are average diameters of ellipsoidal manganese sulfide inclusions; $\bar{a}$ is the average cube edge of titanium carbo-nitride inclusions; $\bar{\lambda}$ is the average center-to-center spacing between inclusions; V_v is the volume fraction of inclusions.

1 and shows the fracture surface to be almost completely covered by large equiaxed dimples approximately 10 to 20 μm in diam. At the positions marked "X" on the fractograph, examples of impressions of shattered carbo-nitride particles may be seen at the bottoms of dimples. Stereoscopic examination of these shattered carbo-nitrides revealed that the pieces fit together much like a jigsaw puzzle. Although a few carbo-nitrides were observed to be cracked in unstrained specimens, no separation of broken pieces nor noticeable clustering of inclusions was observed before straining. The conclusion is that the shattering occurred at small plastic strains and substantial separation of the broken pieces of the carbo-nitrides observed on the fracture surfaces occurred during the fracture process.

The particular carbo-nitride marked "Y" in Fig. 1 exhibits clearly a cleavage fracture pattern, suggesting that the associated dimple was nucleated by the separation of the halves of the fractured non-metallic inclusion. At the position marked "R" in Fig. 1, evidence of surface rumpling of the dimple walls is seen. These wavy, linear features are reminiscent of the intense deformation markings on the free surfaces of tensile specimens which have been strained well into the plastic region. The implication is that the dimple walls were free surfaces during a portion of the plastic deformation of the matrix and that large amounts of plastic deformation occurred after void initiation. This latter point is further substantiated by the large separations observed between pieces of the shattered carbo-nitrides on the maraging fracture surfaces, in many instances representing strains several times the observed macroscopic strains at fracture.

A representative fractograph illustrating the features observed on the AISI 4340 fracture surfaces is presented in Fig. 2. The AISI 4340 fracture surfaces were composed of widely spaced large dimples 5 to 15 μm in diam. (as marked with the letter "L" in Fig. 2) separated by extensive areas of very fine dimples one-to-two orders of magnitude smaller. Both commercial and high-purity AISI 4340 alloys exhibited extensive surface rumpling on the large dimple walls as was observed in the maraging steels. The feature marked "X" within the large dimple in Fig. 2 is the impression of the void nucleating particle. The replicated shapes of these particles were generally ellipsoidal. This observation combined with the fact that the large dimple spacings on the fracture surfaces corresponded with the spacings of the non-metallic inclusions in the AISI 4340 alloys demonstrates that the large dimples were nucleated by manganese sulfide inclusions. Careful examination of a number of the nucleating sulfides at the bottoms of large dimples suggested that the void had been formed by decohesion of the sulfide-matrix interface since no fracture patterns were observed on the nucleating sulfides. Some evidence in the form of deformation markings and steps on the inclusion surfaces suggested that the sulfides had undergone plastic deformation during straining.

Examination of the areas of fine dimples at high magnification showed that many of these small dimples contain the impression of a nucleating particle. The absence of any fracture patterns on these nu-

Fig. 1—Electron fractograph from 18 Ni maraging steel (shattered carbo-nitrides indicated by X; cleavage fracture pattern on carbo-nitride indicated by Y; deformation markings indicated by R).

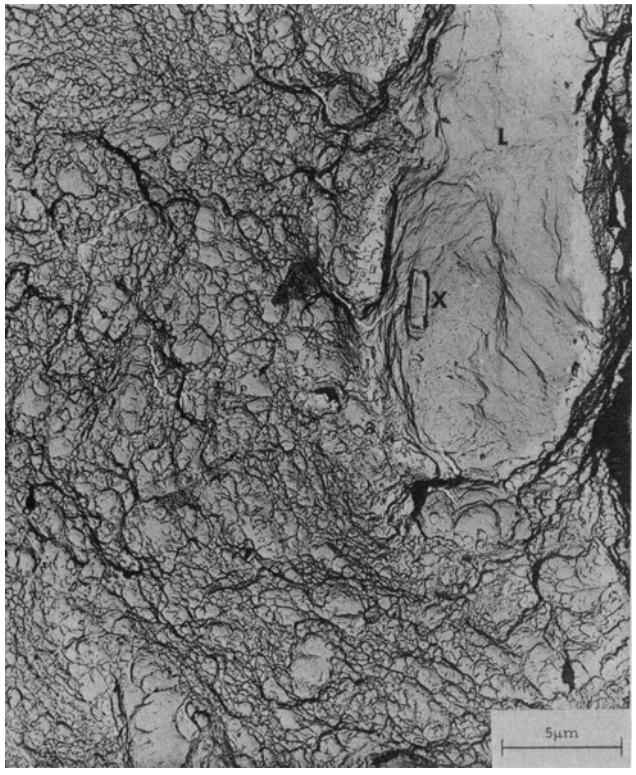

Fig. 2—Electron fractograph from AISI 4340 steel (large dimple indicated by L; nucleating particle indicated by X).

cleating particles suggest that the small voids were nucleated by decohesion of the matrix from the small particles. In order to identify the nucleating particles of the small dimples, a series of extraction replicas were taken from the fracture surfaces of the AISI 4340 alloys and resulted in the extraction of many fine particles associated with the small dimples, as illustrated in Fig. 3 (the arrows indicate extracted particles). Using selected area electron diffraction, these small nucleating particles were found to have the crystal structure of cementite (Fe_3C).

In an attempt to define the fracture paths in these alloys, fractured tensile halves were nickel plated, sectioned longitudinally, and polished to the midplane. Representative micrographs from the AISI 4340 and 18 Ni maraging alloys are presented in Fig. 4. The fracture profile of an AISI 4340 specimen (Fig. 4(*a*)) shows the fracture to be quite irregular and to follow the boundaries of the martensite laths. This observation of the fracture path following the martensitic boundaries is not too surprising since approximately 90 pct of the fracture surface area of each AISI 4340 specimen was covered with small dimples nucleated by cementite which precipitates preferentially at martensite lath boundaries.[11] In contrast, the fracture profiles of the 18 Ni, 200 grade maraging steels, as shown in Fig. 4(*b*), exhibit no apparent tendency of the fracture to follow particular microstructure features.

PROCEDURE FOR INVESTIGATING THE PLASTIC FRACTURE MECHANISM

As discussed above, it was observed that for any one of the four alloys, the fracture features in the region of fast fracture initiation on K_{Ic} specimens were the same as those from the central regions of normal rupture on smooth and mildly notched, round tensile specimen fracture surfaces. These observations lead one to speculate that the mechanisms of plastic fracture are at least qualitatively the same for the three specimen geometries in these particular alloys. While precracked fracture toughness specimens are meant to simulate flawed material in service, they are expensive to produce, and it is generally quite difficult to arrest the fracture process once it has begun, especially in high-strength materials. Thus, it was decided to study the initiation and progression of plastic fracture in smooth and mildly notched, round tensile specimens with the belief, based on the above fractographic observations, that the observed processes would be comparable to those taking place at the tip of a crack.

The dimensions and geometries of the two tensile specimen types are given in Fig. 5 together with their orientation in the plate materials. The particular geometry of the mildly notched or pre-necked specimen was chosen based on the previous work of Sachs[12] in order to assure fracture initiation in the center of the specimen and to closely match the stress and strain states found in the smooth, round specimens. These conditions were desirable in order to determine the effects of increased tensile triaxiality by comparing the observations made with the smooth specimens with those made with the mildly notched specimens.

The general procedure for the metallographic investigation was to load a tensile specimen to some predetermined level of strain (all reference to strain in this paper should be interpreted as: $\epsilon = \ln(R_0^2/R_f^2)$), unload and section the specimen longitudinally, exposing the longitudinal midplane normal to the primary rolling direction to metallographic examination. It was observed on the longitudinal midplanes of fractured tensile specimens that the presence of large voids was not limited to the fracture path, but rather voids extended away from the fracture surfaces in the direction of the tensile axis. To provide measurements which offer an average of stress conditions found in the neck (which vary with position in the neck) yet are pertinent to the fracture process, an area centered on the point of intersection of the minimum diameter of the neck and longitudinal bisector of the specimen was metallographically examined. The dimensions of the area varied from alloy to alloy. These dimensions were chosen with reference to the fractured tensile halves so that the longitudinal dimension of the area extended to include all voids of substantial size away from the fracture surface, and the transverse dimension of the area was taken as the width of the area of normal rupture on the fracture surface, *i.e.*, the shear lips were not included. Within these areas in the centers of the tensile necks, the numbers, sizes, and locations of voids were tabulated for various levels of strain.

VOID INITIATION

As was illustrated above, the fracture surfaces of the 18 Ni, 200 grade maraging steels are composed al-

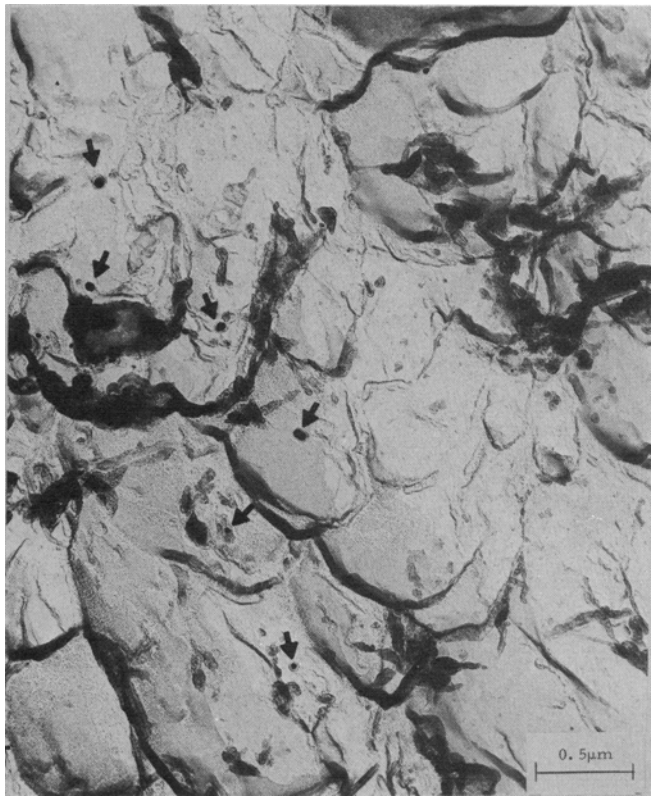

Fig. 3—Extraction replica from fracture surface of AISI 4340 steel (arrows indicate extracted cementite particles).

most entirely of large dimples. The presence of cleaved carbo-nitride inclusions lying in the bottoms of the large dimples together with the good correlation between inclusion spacing in the matrix and the dimple spacing on the fracture surfaces led to the supposition that the dimples (voids) in the maraging steels are nucleated by the carbo-nitride inclusions. The metallographic investigation at 1000X of the series of strained and sectioned tensile specimens confirms this hypothesis. In both high-purity and commercial 18 Ni maraging alloys and for both smooth and notched tensile specimens for which straining was interrupted before fracture, the cracking of carbo-nitride inclusions was observed directly as the exclusive origin of voids in the maraging alloys.

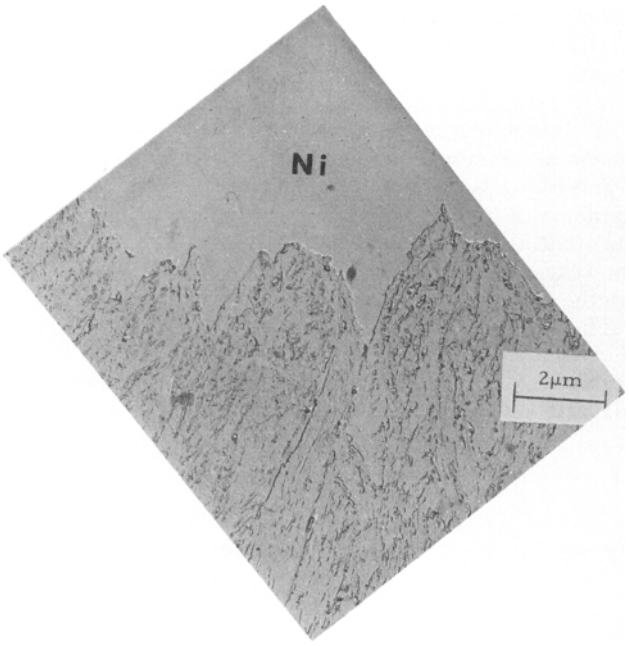

(a)

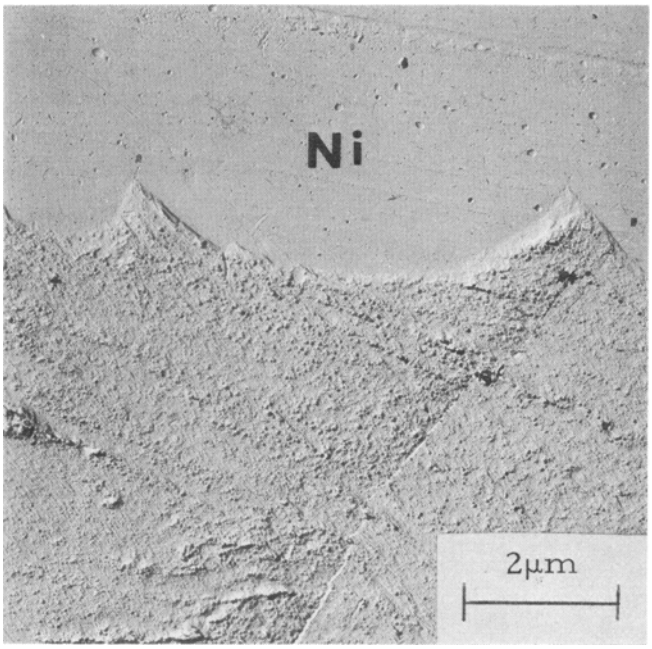

(b)

Fig. 4—Transmission micrographs of replicas from profiles of smooth tension fractures. (*a*) AISI 4340 steel; (*b*) 18 Ni maraging steel.

It was observed that the larger inclusions fractured first, *i.e.*, at lower strains, with the process of cracking continuing as the strain increased with smaller and smaller inclusions beginning to fail. Although some inclusions were fractured before straining, it was the general observation that the cracking of the carbo-nitrides occurred after loading the specimens into the plastic region and at stress levels above 200 ksi (1378 MN/mm^2) which correlates well with the results of Floreen and Hayden.[13]

The fact that the carbo-nitrides fail by cleavage indicates that they are brittle, which was further confirmed by microhardness tests using a Tukon tester with a 136 deg diamond pyramid indentor and 5 g load. Many of the inclusions fractured during indentation with several fragments being dislodged during the shattering of the inclusions. The very brittle nature of the carbo-nitrides provides a basis for an explanation of the observed fact that the larger inclusions fail at lower strains (applied stress). As first developed by Weibull,[14] the fracture strengths of brittle solids depend upon the size of the solid being loaded. Simply put, the argument is that the larger the volume of brittle material, the greater is the probability of finding larger size flaws in the structure which lead to fracture at lower stresses. Although it is impossible to quantitatively apply the statistical approach to the fracture strengths of the carbo-nitride inclusions in the maraging steels for lack of sufficient data, the Weibull theory does qualitatively predict that the larger the inclusion, the lower the stress at which it will fail.

In order to study quantitatively the void initiation process, the number of inclusions present in the central areas of the strained tensile specimens were counted together with the number of voids present and the number of inclusions with associated voids, *i.e.*, cracked inclusions and those associated with well developed voids. These tabulations permitted

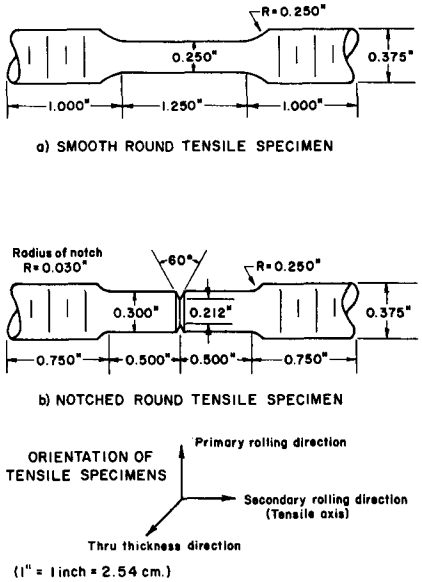

Fig. 5—Shapes and orientation of tensile specimens

calculation of the percent of inclusions which have voids associated with them at each level of strain, a quantity which is a measure of the extent of void nucleation. The results for the percent of inclusions in the maraging steels which had voids associated with them are presented in Fig. 6.

These plots indicate that void initiation is a continuous process with increasing strain. Note that in the commercial grade steel, 19.3 pct of the carbonitrides were fractured before any load was applied. The largest inclusions present were generally the ones which were fractured in the as-received condition. At any given level of strain, the percentage of inclusions with voids was larger for the commercial grade alloy, undoubtedly due to the larger size inclusions in the commercial alloy. Also, the percentage of inclusions with voids at a given strain was much larger in the notched specimens than in the smooth, and the rate of void initiation was much greater for the notched specimens.

The differences between the behavior in the smooth and notched specimens could be due to either the higher level of applied stress in the notched specimens at any given strain or to the greater level of tensile stress triaxiality found in the notched specimens. To illustrate these points, consider the stress-strain curves for the commercial purity 18 Ni maraging steel presented in Fig. 7. The solid curves represent the stress-strain relationships determined using single specimens loaded to fracture (solid data points), while the open data points represent the stress and strain conditions of interrupted tests which were subsequently sectioned for metallographic examination. As can be seen in the figure, the data from the interrupted test specimens fall on the same stress-strain curves, assuring that the specimens all have the same flow characteristics. This same observation was also made for all other alloys in this investigation. Also included in Fig. 7 is the uniaxial flow curve (dashed curve) as determined using the Bridgman correction for necking.[15] At any given strain, the differences between the solid curves and the uniaxial flow curve roughly correspond to the levels of triaxial tension in the specimens. Thus, as may be readily seen in Fig. 7, at any given strain the level of applied stress and the level of triaxial tension are much greater in a notched specimen than in a smooth.

By plotting the percentage of inclusions with voids against the applied tensile stress, as in Fig. 8, it was found that the data for both smooth and notched specimens fall on the same curve for each alloy. Since the level of triaxiality varies from smooth to notched specimen at any level of applied stress, Fig. 8 demonstrates that the level of tensile stress triaxiality has no measurable effect on void nucleation in these maraging alloys. Rather, void nucleation is dependent upon the level of applied tensile stress.

The fracture surfaces of the AISI 4340 alloys were shown above to be covered by two populations of dimples. Good correlation between the spacings of manganese sulfide inclusions in the matrix and large dimple spacings on the fracture surfaces together with examples of characteristic inclusion impressions in the dimples led to the supposition that the large dimples on the fracture surfaces of the AISI 4340 were nucleated by manganese sulfide inclusions. The results of the metallographic study of strained and sectioned tensile specimens confirms this hypothesis. It was observed that the large voids are initiated almost exclusively by separation of the sulfide-matrix interface in both specimen types in the AISI 4340 alloys.

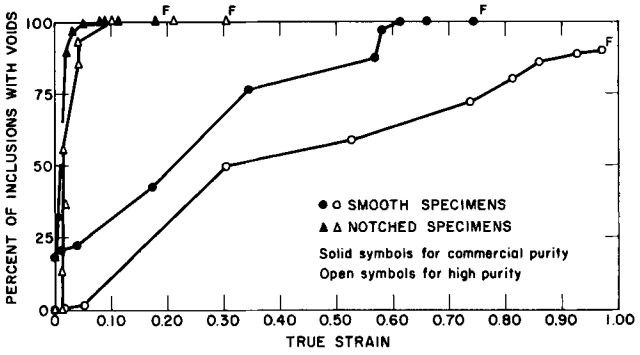

Fig. 6—Pct of inclusions with voids as a function of true strain for 18 Ni maraging steel ("F" indicates value taken from only one-half of a fractured specimen).

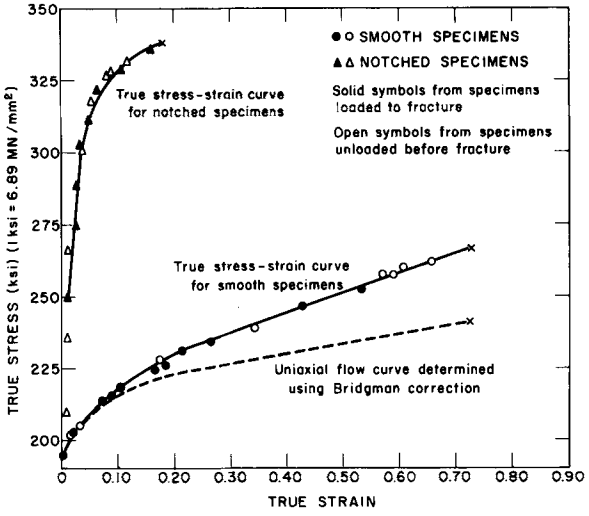

Fig. 7—Tensile curves for commercial purity 18 Ni maraging steel.

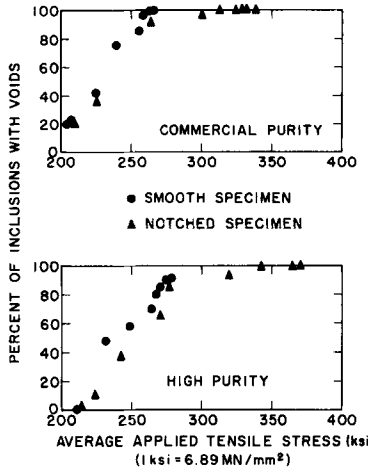

Fig. 8—Pct of inclusions with voids as a function of applied tensile stress for 18 Ni maraging steel.

As was observed for the 18 Ni maraging steels, in this case also the largest inclusions nucleate voids first, *i.e.*, at lower strains. As straining proceeded, smaller and smaller inclusions would then begin to nucleate voids so that the nucleation process was continuous as strain increased with progressively smaller inclusions acting as nucleating sites for voids. No void initiation at the sulfide-matrix interface was observed unless the matrix had flowed plastically.

Chao and Van Vlack[16,17] have shown that deformation is concentrated in manganese sulfide particles which are embedded in a ferrous matrix during straining. Furthermore, Van Vlack *et al.*[18,19] report that plastic deformation in manganese sulfide occurs by planar slip which results in straight slip steps on suitably oriented free surfaces as confirmed in this investigation by micro hardness indenting numerous sulfides in the AISI 4340 alloys. These observations provide a possible explanation for the observed effects of inclusion size on nucleation of the large voids in the AISI 4340 alloys. As the material is loaded, more plastic deformation occurs in the manganese sulfide inclusions than in the matrix. Planar slip provides rather long, narrow slip bands within the inclusions which are blocked at the inclusion-matrix interface, resulting in substantial stress concentration across the boundary and resultant fracture there. Zener[20] has shown that the local stress at the tip of a blocked slip band is proportional to the square root of the length of the band. The average length of slip band is obviously related to the size of the manganese sulfide. This treatment predicts that the local stress at the boundary increases with the size of the sulfide; and thus the boundaries at the larger inclusions should fail first, as has been observed.

The strained and sectioned specimens of AISI 4340 were examined metallographically at 1000X, and the percentage of inclusions with voids in the central regions of the specimens were recorded at various strains. The results are plotted in Fig. 9. The curves indicate that the initiation process is continuous as straining proceeds until the specimen fractures or all of the inclusions have nucleated voids. Note that, by comparison with Fig. 6, the strains to fracture for both are much lower for the smooth and notched tensile specimens than for both maraging steels. The data show that in the commercial purity alloy, voids are initiated at lower strains than in the high-purity, and the slopes of the plots in Fig. 9 indicate that the rate of void initiation is higher for the commercial purity AISI 4340. Both of these observations are undoubtedly the result of the larger sizes of inclusions found in the commercial steel. The percentage of voids at a given strain and the rates of void nucleation for the notched specimens are much greater than for the smooth. This fact is again due to the higher stresses in the notched specimens at a given strain. It was found that the data for both smooth and notched specimens fell on the same curve when plotting the percentage of inclusions with voids against the applied tensile stress indicating, as was observed for the maraging steels, that there is no effect of stress triaxiality on void initiation.

While it was previously established that the small dimples on the fracture surfaces of the AISI 4340 steels are nucleated by cementite particles, it is of interest to know exactly how the small voids are nucleated. Although the nature of the impressions of the carbide particles on the fracture surfaces point to a mechanism of interface failure, since they exhibit no fracture pattern within themselves, the point is not conclusively decided by fractography. In order to establish the exact mechanism of void nucleation at the carbides, a series of thin foils were prepared from near the fracture surfaces of broken AISI 4340 specimens. Evidence was found, using the electron microscope, that the small voids in the AISI 4340 steels are nucleated by decohesion of the carbide-matrix interface. Fig. 10 presents two observed examples of voids formed by separation of the carbide-matrix interface. The voids are indicated by the arrows, and the carbides by the letter "C". Selected area electron diffraction confirmed these particles to be cementite.

VOID GROWTH

As the stresses are increased beyond the levels at which void nucleation first occurs in these alloys, the voids which have been initiated at non-metallic inclusions grow by some mechanism involving plastic flow of the matrix. Examination of the midplanes of many strained and sectioned tensile specimens re-

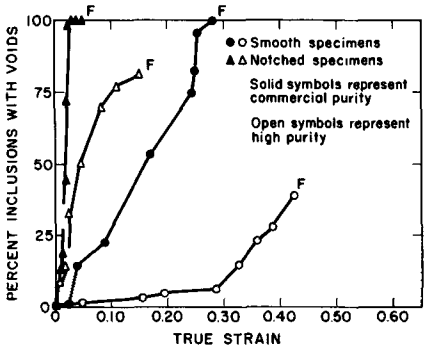

Fig. 9—Pct of inclusions with voids as a function of true strain for AISI 4340 steel ("F" indicates value taken from only one-half a fractured specimen).

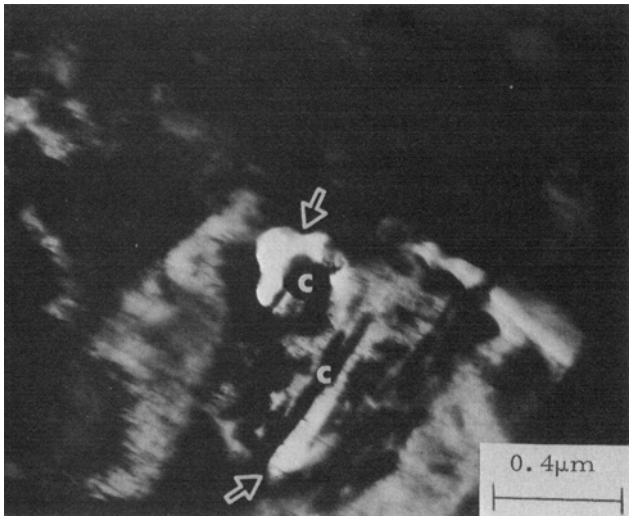

Fig. 10—Void initiation by decohesion of carbide-matrix interface in AISI 4340 steel strained plastically (arrows indicate voids and "C" indicates carbide).

vealed that there is a progressive increase in both the number and size of voids in the necked regions of both smooth and notched specimens of both alloys as the strain is increased. The increase in the number of voids as the strain increases is the result of continuing void initiation at smaller and smaller inclusions, while the increasing size of voids is the result of progressive void growth. These two simultaneously occurring processes result in a wide spread in the sizes of voids present on the longitudinal midplanes.

It was observed for both alloys that the larger voids were located in the centers of the specimens, with the sizes of voids generally decreasing as one moves away from the center line. The general shapes of the voids also change from edge to center of the midplane at high strains. In the centers of the smooth specimens and more generally in the notched specimens, the voids show a tendency to grow in both the direction of the tensile axis and in the radial direction (perpendicular to the tensile axis). Examples of

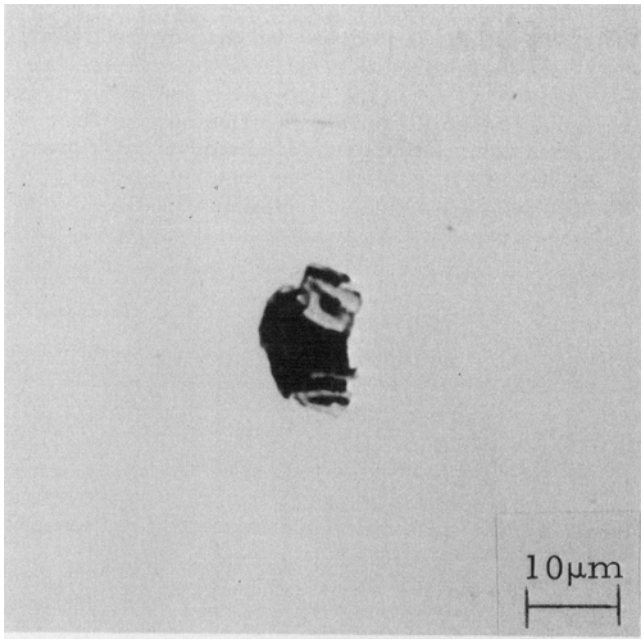

(a)

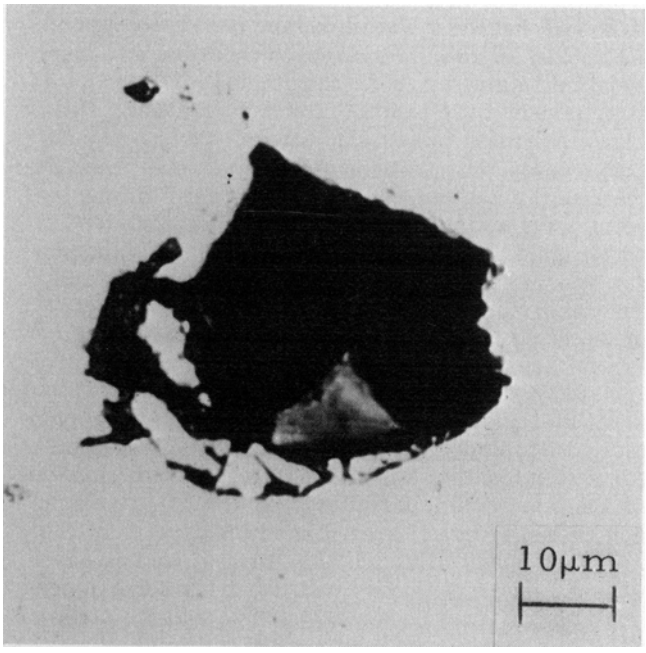

(b)

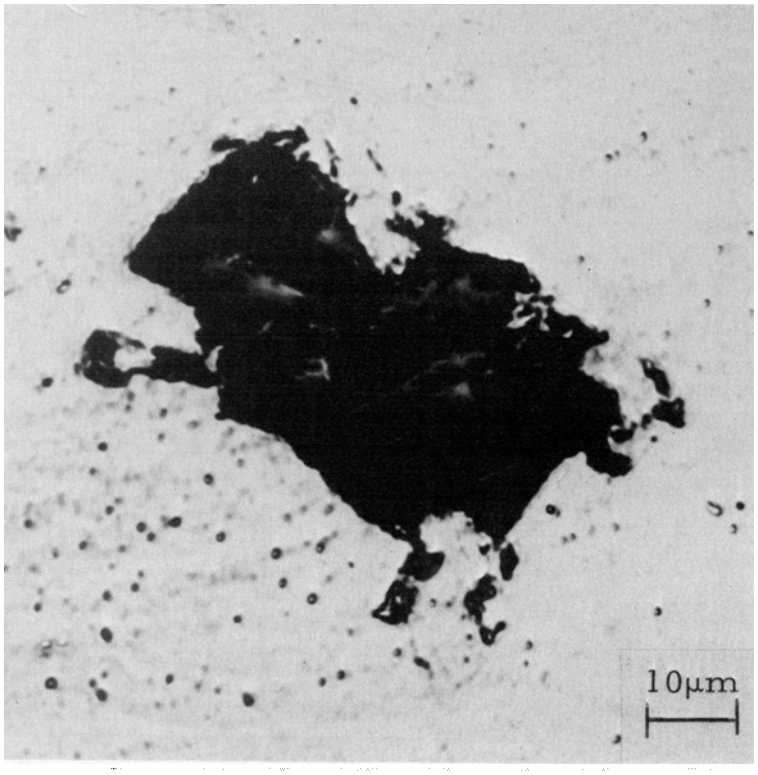

(c)

Fig. 11—Voids in the centers of tensile specimens of 18 Ni maraging steels strained various amounts plastically. (*a*) $\epsilon = 0.18$; (*b*) $\epsilon = 0.58$; (*c*) $\epsilon = 0.66$.

voids in the central portions of the tensile specimens which have grown during straining are presented in Fig. 11. (The examples in Fig. 11 are from specimens of 18 Ni maraging steel, but these same observations were also made for the AISI 4340.)

It should be noted that at small strains (Fig. 11(*a*)), the voids in the center of the specimen showed little sideways growth, rather they tend to grow preferentially in the direction of the applied tensile stress. However, as the strain increases (Fig. 11(*b*) and 11(*c*)), the voids in the central region of the neck grow both longitudinally and laterally. It was also observed that the voids which are nucleated outside the necked region, *i.e.*, removed from the minimum specimen diameter in the longitudinal direction, tend to show little lateral growth even at high strains. Likewise, voids toward the edges of the specimens also showed little tendency for appreciable growth in the radial direction even at high strains. These voids lying away from the center of the neck tend to be elongated in the direction of the tensile axis and are generally no wider than the nucleating particle. The larger degree of triaxial stress in the center of the neck which develops at high strains aids the lateral growth of the voids.

Using a standard point counting technique,[21] it was possible to determine the area fractions of the longitudinal midplanes covered by voids. Using this information together with the number of voids present on the test section permitted calculation of the average cross-sectional area of void intersected by the midplane. This particular measure of void size was chosen since it was observed that the voids are generally quite irregular in shape such that the measurement of some linear dimension of the voids, *e.g.*, length or width, has questionable utility.

The values of the average cross-sectional areas of voids intersected by the midplanes as a function of strain are presented in Fig. 12. Each of the curves in the figure shows a linear initial portion where the average size of void increases continuously with strain. At the higher levels of strain, the curves (especially those for the smooth specimens) show a rapid increase in the size of voids present. This rapid jump corresponds with the onset of void coalescence and the formation of a large central cavity in the tensile specimen. It should be noted that the rates of void growth are generally higher for the commercial grade alloys and noticeably higher for the notched specimens.

Actually, the average cross-sectional area of void represents the combined effects of void nucleation, growth, and coalescence such that the plots in Fig. 12 represent some measure of the progress of the total fracture process. These results do indicate that at any given strain, the most detrimental situation is found in the notched commercial grade AISI 4340 steel while the least damaging situation is found in the smooth high-purity grade 18 Ni maraging steel. The general order of the curves follows the observed values of fracture strain and fracture toughness in these alloys.

In order to separate the effects of void nucleation and growth, the cross-sectional area of the largest void present on the midplane was determined. The reasoning behind this choice is that the largest void present would naturally be the one which had nucleated first (at the largest inclusion) and had grown continuously as the strain had increased, and thus represents the best available information regarding void growth. The areas of the largest voids were used to calculate the radii of circles of equivalent areas, values of which are plotted against strain for all the alloys in Fig. 13. Only values observed before void coalescence began are plotted. The values observed for the maraging steels agree reasonably well with those observed by Floreen and Hayden for an 18 Ni, 300 grade maraging alloy.[22]

The data in Fig. 13 indicate that for any given alloy the rate of void growth is greater in the commercial-purity material than in the high-purity material. This fact is due to the differences in inclusion size when going from commercial-purity to high-purity alloys. As may be seen in Table III, the center-to-center distances between inclusions ($\bar{\lambda}$) are larger in the

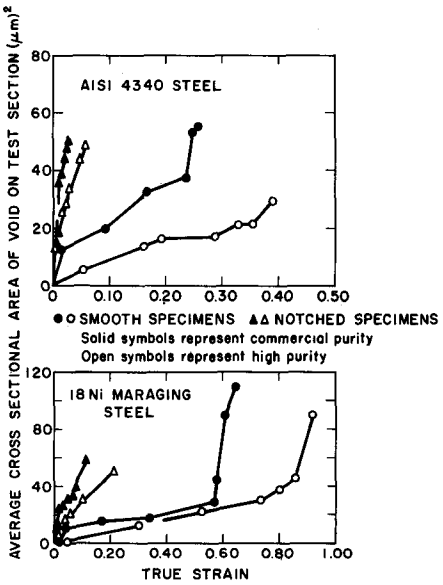

Fig. 12—Average cross sectional area of void as a function of strain.

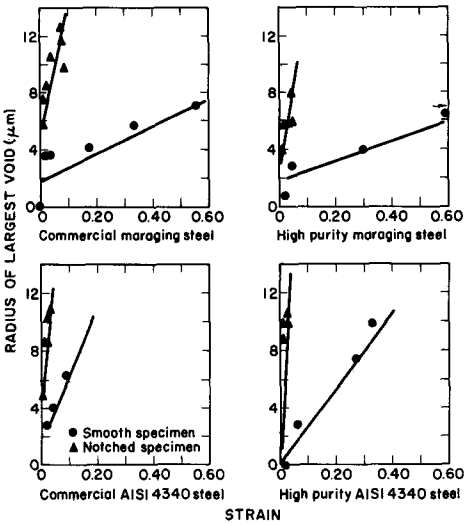

Fig. 13—Radii of largest voids as a function of strain.

commercial-purity alloys. However, if the differences in the sizes of the inclusions between high-purity and commercial purity alloys are considered, it is seen that the boundary-to-boundary distances between nearest neighbor inclusions are roughly the same for both purity levels in a given steel. Once voids nucleate at neighboring inclusions, they have approximately the same amount of growth in the matrix required before impingement in both commercial and high-purity alloys. Thus, the primary difference between the alloys regarding growth of voids stems from the fact that the voids nucleate earlier in the commercial steels since the inclusions are larger; and because the inclusions are larger, the resulting voids are born larger which produces increased levels of applied stress due to the reduced cross-sectional area and interaction of the stress fields around the voids. With the increased levels of local stress in the commercial alloys, the voids grow more rapidly. These findings regarding the detrimental effects of inclusion size are supported by the recent work of Darlington[23] who studied fracture in electrolytic iron and spheroidized low carbon steel.

The results presented in Fig. 13 also demonstrate that the increased level of triaxial stress introduced in the notched specimens greatly increases the rate of void growth. At a given level of strain, the uniaxial flow stress (which is twice the maximum resolved shear stress) is the same in both smooth and notched specimens of a given alloy, as shown in Fig. 7, yet the sizes of the voids are much larger in the notched specimens and the rate of void growth is greater. This difference in void growth must then be the result of the difference in the level of triaxiality.

Increased levels of triaxiality increase the longitudinal applied stresses required to cause general plastic flow in the matrix. Restricted flow in the matrix will tend to concentrate the plastic deformation at the existing voids where the stresses are highest and constraints reduced, since the stresses normal to the free surfaces of the voids go to zero. Thus, the maximum shear stress increases near the surface of a void (since one of the principal normal stresses is zero) resulting in increased plastic deformation. Hence, as the level of triaxiality increases, the higher applied longitudinal stresses necessary to continue plastic flow result in intense deformation around the voids resulting in enhanced rates of void growth.

There have been several attempts to describe the void growth process in the past. Many of the treatments involved expressions for predicting void size from the strain. However, for several of the cases,[24,25] it is difficult to compare the results of the current investigation with those predicted because the treatments contain various arbitrary constants which are used to make the data fit models. On the other hand, the work of Rice and Tracey[26] involves complex expressions of strain rate which are not readily integrated for comparison with the current data. The analyses to which the data from this investigation may be most readily compared are those of McClintock,[26,27] which are based on continuum plasticity and involve no arbitrary constants. McClintock considers an isolated hole in a matrix with the shape of a right prism of elliptical cross-section. Using the expression developed by McClintock and the values of the various materials constants for the alloys being investigated here, the observed void sizes were compared with those predicted. In all cases the observed values were at least twice those predicted by the McClintock analysis. The poor agreement probably results from the fact that the McClintock analysis assumes no interaction between voids, *i.e.*, it should be valid only for the very early stages of void growth and for systems with much larger spacings between inclusions than those encountered in these structural alloys.

VOID COALESCENCE

As was suggested by examination of the fracture surfaces of the 18 Ni maraging steels which were covered with large dimples centered on fractured carbo-nitride inclusions, the metallographic examination of strained and sectioned specimens of the maraging alloys demonstrated that the inclusion-nucleated voids coalesce by growing until they impinge on one another. The first appearance of the coalescence of voids in both the high-purity and commercial maraging steels was observed to occur at strains of approximately 0.8 of the fracture strains for the smooth specimens and between 0.4 and 0.6 of the fracture strains for the pre-notched specimens. An example of voids coalescing in the maraging steel is presented in Fig. 14. As straining continues, the void coalescence process leads to the formation of a large cen-

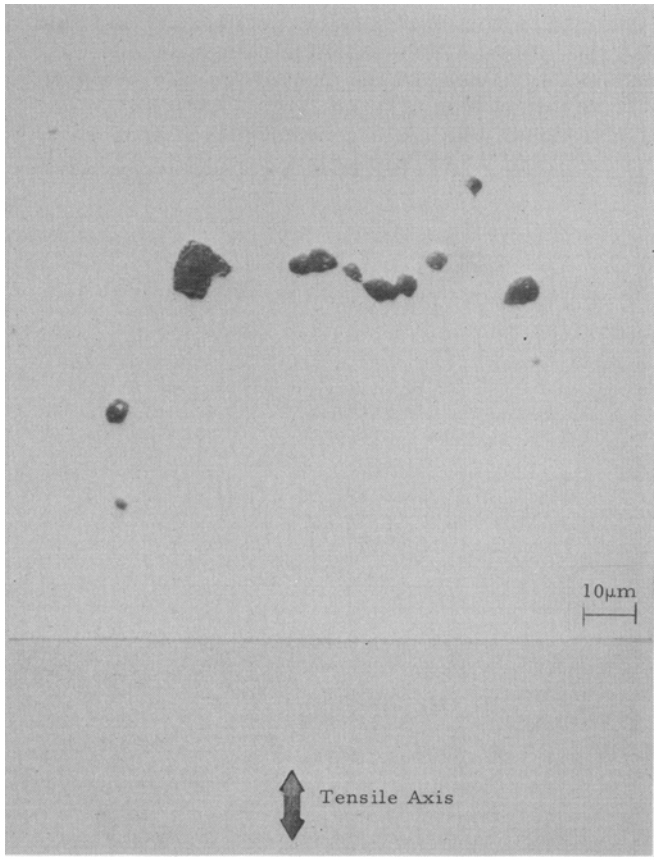

Fig. 14—Void coalescence in 18 Ni maraging steel, $\epsilon = 0.81$.

tral cavity. Once a cavity as long as 5 to 10 pct of the minimum specimen diameter was formed, final fracture occurred very rapidly.

This same process of void coalescence was observed in the notched specimens. It was generally observed that the strains at which the coalescence of voids was first detected were smaller in the notched specimens, approximately 20 pct of those observed in the smooth specimens, which results in the fact that the fracture strains of the notched specimens are substantially less than those of the smooth specimens. This early development of coalescence obviously follows from the higher void growth rates observed in the notched specimens. Furthermore, the duration of the coalescence process, *i.e.*, the difference between the strain at which coalescence is first detected and the fracture strain, was found to be much shorter in the notched specimens, of the order of half the values noted for the smooth specimens. The foreshortened coalescence stage of the voids in the notched specimens must also be a direct result of more rapid growth under the influence of the higher triaxial stresses.

Thus far, it has been seen that at least qualitatively the process of void initiation and growth from nonmetallic inclusions in the two alloy steel families (maraging and quenched and tempered) are not essentially different. However, the process of the coalescence of inclusion-nucleated voids in the AISI 4340 alloys differs dramatically from that in the maraging steels. One would expect as much after considering the fracture surfaces of the quenched and tempered steels which are covered by two distinct populations of dimples. Based on observations made from the strained and sectioned tensile specimens, it is found that the large voids nucleated at manganese sulfide inclusions coalesce by the propagation of crack-like features which link adjacent large voids. The first appearance of this coalescence occurs at approximately 0.6 to 0.8 of the fracture strain for the smooth specimens and approximately 0.3 to 0.4 of the fracture strain for the notched specimens. A photomicrograph of the coalescence of inclusion-nucleated voids in AISI 4340 is presented in Fig. 15. At strains within a few percent of the fracture strain, the coalescence of voids in the central region of the tensile specimen is extensive enough to form a rather large continuous cavity spanning as much as 5 or 10 pct of the specimen diameter. Final fracture occurs catastrophically after this point.

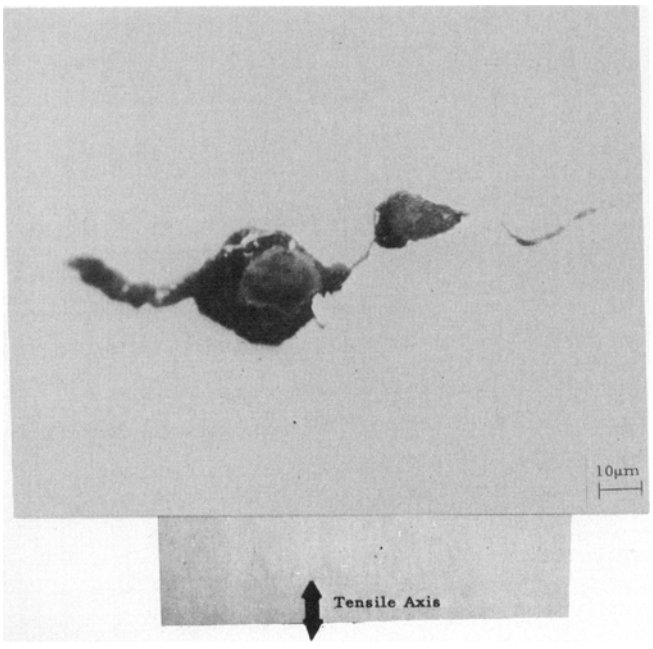

Fig. 15—Void coalescence in AISI 4340 steel, $\epsilon = 0.25$.

The crack-like features which link the large inclusion-nucleated voids in the AISI 4340 alloys initially have the appearance of a collection of small voids similar to the "void sheets" described by Rogers[29] which he observed during the plastic fracture of copper. This fact is readily seen in the example presented in Fig. 16(*a*). As the strain is increased, the small voids coalesce and the "void sheet" becomes an actual crack of substantial opening, running between the large voids, as demonstrated in Fig. 16(*b*). Serial sectioning of several of these "void sheets" conclusively demonstrated that they are planar features, generally oriented at approximately 45 deg with the tensile axis, composed of many small voids.

The metallographic observations lead to the conclusion that the voids nucleated by the manganese sulfides grow to some critical size or until a critical spacing between them is reached. At this point, further deformation seems to be concentrated in the narrow bands between the neighboring large voids. As straining continues, the bands of intense deformation between the voids become more distinct and the small voids formed at the carbide particles in these bands begin to coalesce, resulting in the formation of a "void sheet" and subsequent crack connecting neighboring large voids.

If it is assumed that the nucleation of small voids at the carbide precipitates could be avoided without affecting the rates of growth of the inclusion-nucleated voids, as determined from Fig. 13, it is possible to ascertain whether or not improvement in the strains to fracture could be realized. Using half the average inter-inclusion spacing as the approximate radius of the large voids at fracture if void sheet formation were avoided and the slopes (growth rates) from Fig. 13, the predicted fracture strains for the AISI 4340 alloys are considerably higher than those observed in practice. For example, the observed fracture strain for smooth specimens of the high-purity alloy was 0.52 and the predicted fracture strain, assuming no void sheet formation is 0.90. Although this treatment is highly problematic since changing the carbide distribution to avoid the nucleation of small voids will undoubtedly change the flow characteristics of the matrix, it does indicate that improvement in the resistance to plastic fracture can follow from restricting the formation of void sheets which result in the premature coalescence of the inclusion-nucleated voids.

This premature coalescence in the AISI 4340 alloys also explains the observed differences in toughness between the AISI 4340 alloys and the 18 Ni, 200 grade maraging steels. The particles of intermetallic compound which strengthen the maraging steels are one to two orders of magnitude smaller than the carbides

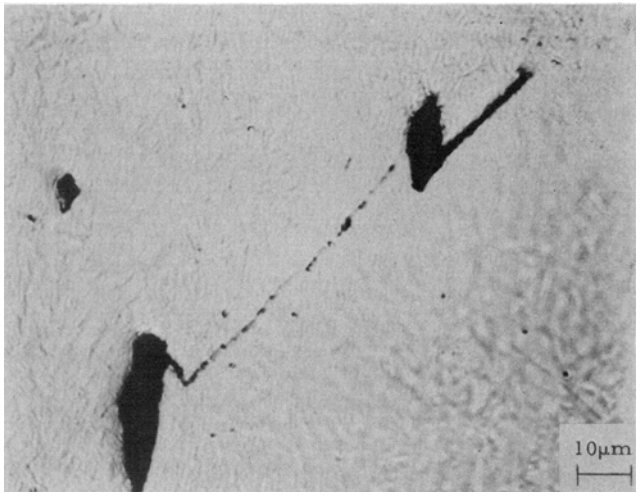

(a)

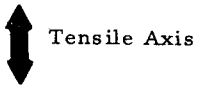

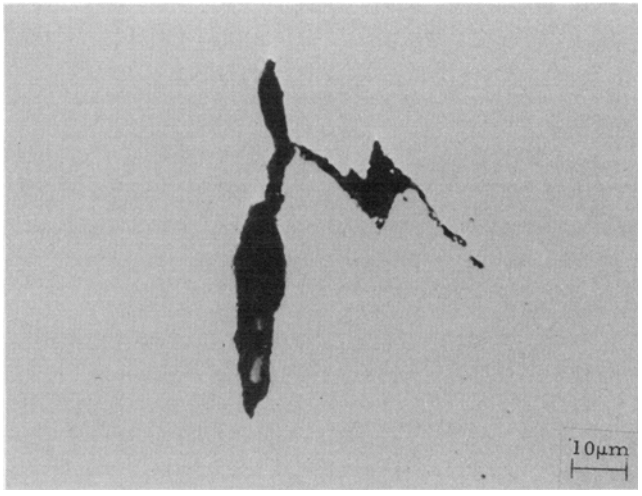

(b)

Fig. 16—Coalescence of voids by void sheet formation in AISI 4340 steel strained plastically. (*a*) $\epsilon = 0.25$; (*b*) $\epsilon = 0.27$.

in the quenched and tempered steels. Roesch and Henry[30] have demonstrated that these strengthening precipitates in the maraging alloys do nucleate voids when they are coarsened and this results in a concurrent drop in toughness as measured by impact energies. These observations suggest that it may be possible to prevent or delay the nucleation of voids at the cementite particles by suitably refining the carbides in the quenched and tempered structure, thereby improving the fracture toughness.

SUMMARY OF RESULTS

The microstructural aspects of the plastic fracture processes in AISI 4340 and 18 Ni, 200 grade maraging steels have been defined by studying strained and sectioned, smooth and notched, tensile specimens together with the fracture surfaces of tensile and fracture toughness specimens. The interruption of the growth of the inclusion-nucleated voids in the quenched and tempered AISI 4340 steels by the formation of void sheets is the primary reason that the quenched and tempered steels are generally less tough than the maraging steels at the same strength level. It was observed that void nucleation occurs at lower strains at the large inclusions and that void growth takes place more rapidly from the larger inclusions, thus reducing the resistance of the alloy to fracture. By comparing the metallographic results from smooth and notched tensile specimens, it was demonstrated that void initiation is independent of the level of tensile stress triaxiality, but that void growth rates are increased substantially by increasing the level of triaxial tension. Increased growth rates result in more rapid coalescence of voids and premature fracture, explaining the mechanism by which notches and flaws in high strength structural materials lead to brittle fractures even when the microscopic fracture mode is dimpled rupture (plastic fracture).

The investigation indicates that the most important microstructural features governing the plastic fracture of these alloys are the void nucleating, second-phase particles. The toughness of these alloys may be most readily improved by decreasing the number and size of non-metallic inclusions. Although recently reported work by other investigators[31-33] indicates that at high strength levels (250 to 320 ksi) fracture toughness is insensitive to steel cleanliness, the frac-

ture mode exhibited at these high strength levels in severely notched K_{IC} specimens is mixed, consisting of plastic fracture and cleavage[31] and thus the results reported herein are not directly applicable.

Thus far, the approach taken to improve the fracture toughness of the high strength steels has been to use special melting practices to reduce the levels of impurity elements. The practices employed to produce the higher purity levels are generally quite expensive and add substantially to the cost of the final product. The current investigation suggests that inclusion size is an important factor in the fracture process; and that if the average size of inclusions were reduced at any given level of cleanliness, improvements in toughness could be realized. As observed for the manganese sulfide particles, these particles frequently nucleate on deoxidation products present in the melt. This observation suggests that it might be possible to suitably seed or otherwise increase the nucleation of inclusions for a given impurity level of a melt in order to produce a finer dispersion of non-metallic inclusions in the final product. Thus, it might be possible to attain adequate toughness with higher impurity levels provided the sizes of inclusions were reduced.

As the quenched and tempered steels are generally of lower alloy content than the maraging steels and hence more economically produced, it would be beneficial to investigate means of improving their toughness in relation to the maraging steels. As pointed out in the current investigation, the major difference in the fracture behavior of these two different types of steels is the void sheet process of coalescence of inclusion-nucleated voids observed in the AISI 4340 alloys. The voids of these sheets are nucleated by the coarse cementite particles which precipitate at the martensite lath boundaries. It is felt that by refining the size of the carbides and dispersing them more generally throughout the matrix, void initiation at the carbides could be delayed or avoided with a resultant improvement in toughness. Both thermomechanical treatments[34] and repetitive austenitizing treatments[35] have the ability to refine the carbide nucleation during tempering. An investigation of the effects of these treatments on the structure and fracture behavior of AISI 4340 would be helpful for our understanding of the plastic fracture process in the quenched and tempered steels.

ACKNOWLEDGMENTS

The findings presented herein were part of a dissertation submitted by T. B. Cox in partial fulfillment of the requirements for the degree of Doctor of Philosophy at the Carnegie-Mellon University. This research was sponsored by the National Aeronautics and Space Administration under Research Grant NGR 39-087-003.

REFERENCES

1. J. R. Low, Jr.: *Prog. Mater. Sci.*, 1963, vol. 12, no. 1, pp. 1-96.
2. C. P. Sullivan: *Welding Research Council Bulletin* No. 122, 1967.
3. B. I. Edelson and W. M. Baldwin, Jr.: *Trans. ASM*, 1962, vol. 55, pp. 230-50.
4. A. G. Franklin and W. J. McG. Tegart: *J. Iron Steel Inst.*, 1964, vol. 202, pp. 588-92.
5. A. J. Birkle, R. P. Wei, and G. E. Pellissier: *Trans. ASM*, 1966, vol. 59, pp. 981-90.
6. R. Kiessling and N. Lange: *Non-Metallic Inclusions in Steel, Part II*, p. 97, Iron and Steel Institute, London, 1966.
7. T. Boniszewski and E. Boniszewski: *J. Iron Steel Inst.*, 1966, vol. 204, pp. 360-65.
8. R. T. DeHoff and F. N. Rhines: *Quantitative Microscopy*, p. 128, McGraw-Hill, New York, 1968.
9. R. T. DeHoff and F. N. Rhines: *Trans. TMS-AIME*, 1961, vol. 221, pp. 975-82.
10. F. C. Hull and W. J. Houk: *Trans. AIME*, 1953, vol. 197, pp. 565-72.
11. A. J. Baker, F. J. Lauta, and R. P. Wei: *ASTM STP No. 370*, 1965, pp. 3-28.
12. A. W. Dana, E. L. Aul, and G. Sachs: *NACA Tech. Note No. 1830*, Cleveland, Ohio, 1949.
13. S. Floreen and H. W. Hayden: *Met. Sci. J.*, 1970, vol. 4, pp. 77-80.
14. W. Weibull: *Igeniors Vetenskaps Akadamien*, Hondlinger No. 151, Stockholm, 1939.
15. P. W. Bridgman: *Large Plastic Flow and Fracture*, p. 9, McGraw-Hill, New York, 1952.
16. H. C. Chao and L. H. Van Vlack: *Trans. TMS-AIME*, 1965, vol. 233, pp. 1227-31.
17. H. C. Chao and L. H. Van Vlack: *Mat. Res. Stan.*, 1965, vol. 5, pp. 611-13.
18. L. E. Wood and L. H. Van Vlack: *Trans. ASM*, 1963, vol. 56, pp. 770-72.
19. H. C. Chao, L. Thomassen, and L. H. Van Vlack: *Trans. ASM*, 1964, vol. 57, pp. 386-98.
20. C. Zener: *Elasticity and Anelasticity*, p. 133, University of Chicago Press, Chicago, 1948.
21. E. E. Underwood: *Quantitative Stereology*, p. 29, Addison-Wesley, Reading, Mass., 1970.
22. S. Floreen and H. W. Hayden: *Scripta Met.*, 1970, vol. 4, pp. 87-94.
23. H. Darlington: *Ductile Fracture Under Axisymmetric Stresses in Electrolytic Iron and Spheroidized Low-Carbon Steel*, Ph.D. Thesis, Lehigh University, 1971.
24. J. Gurland and J. Plateau: *Trans. ASM*, 1963, vol. 56, pp. 442-54.
25. P. Feltham and A. S. Beyron: *Phil. Mag.*, 1966, vol. 13, pp. 311-16.
26. J. R. Rice and D. M. Tracey: *J. Mech. Phys. Solids*, 1969, vol. 17, pp. 201-17.
27. F. A. McClintock: *Ductility*, p. 255, ASM, Metals Park, Ohio, 1968.
28. F. A. McClintock: *J. Appl. Mech.*, 1968, vol. 35, pp. 363-71.
29. H. C. Rogers: *Trans. TMS-AIME*, 1960, vol. 218, pp. 498-506.
30. L. Roesch and G. Henry: *ASTM STP 453*, 1969, pp. 3-35.
31. J. J. Hauser and M. G. H. Wells: Air Force Mat. Lab. Tech. Rep. AFML-TR-69-339, 1970.
32. J. J. Hauser, M. G. H. Wells, and I. Perlmutter: *J. Vac. Sci. Tech.*, 1972, vol. 9, p. 1339.
33. L. F. Porter: *J. Vac. Sci. Tech.*, 1972, vol. 9, pp. 1340-44.
34. M. J. May and D. J. Latham: *Toward Improved Ductility and Toughness*, p. 157, Climax Molybdenum Development Company, Japan, 1971.
35. R. A. Grange: *Trans. ASM*, 1966, vol. 59, pp. 26-48.
36. D. Broek: *Eng. Fract. Mech.*, 1970, vol. 1, pp. 691-95.